IZM-7: A new stable aluminosilicogermanate with a promising catalytic activity

Elsy El Hayek[a,b], Sambhu Radhakrishnan[b,c], Gina Vanbutsele[b], Sreeprasanth Pulinthanathu Sree[b], Mickaël Rivallan[a], Emmanuel Soyer[a], Christophe Bouchy[a], Eric Breynaert[b,c], Johan Martens[b*], Céline Chizallet[a*], Bogdan Harbuzaru[a]

[a] IFP Energies nouvelles, Rond-point de l'échangeur de Solaize, 69360, Solaize, France.

[b] Center for Surface Chemistry and Catalysis – Characterization and Application Team (COK-KAT), KU Leuven, Celestijnenlaan 200F, 3001 Leuven, Belgium.

[c] NMRCoRe, KU Leuven, Celestijnenlaan 200F – box 2461, B-3001 Leuven, Belgium.

Abstract: Owing to their extra-large pores compared to traditional aluminosilicate zeolites, silicogermanates could be attractive for the catalytic transformation of bulky molecules, provided the frameworks can be modified to incorporate acid sites and can be stabilized to survive calcination. Post-synthetic isomorphic substitution of Ge by Si and Al would present a route to achieve this goal. This report describes the transformation and characterization of the non-stable IM-12 silicogermanate into a new stable IZM-7 aluminosilicogermanate by partially substituting Ge by Si in gaseous form to stabilize the material, followed by an aqueous alumination step. IZM-7-based catalyst presents promising performance in the hydroconversion of *n*-decane compared to conventional zeolites, opening perspectives for the catalytic use of stable derivatives of silicogermanate zeolites.

Keywords: zeolite, silicon tetrachloride, silicogermanate, bifunctional catalysis

Introduction

Zeolites are microporous crystalline aluminosilicates containing pores matching the dimensions of common reactants. Confinement effects explain their impact on chemical reactions [1]. The diversity of zeolites makes them interesting for ion exchange, catalysis, adsorption and separation covering a large scale of applications from biomedical [2] to renewable energies [3,4]. Another interesting family of zeolite-like materials are the silicogermanates [5,6]. Unlike the majority of aluminosilicates, this family benefits from having large to extra-large micropores [7–9] making it *a priori* interesting for the conversion of bulky molecules. However, after removing the organic templates by calcination, most of these silicogermanates lose their crystallinity because of the hydrolysis of the Ge-O bonds. To overcome this instability, preventing their practical applications, post-treatments have been developed to substitute Ge by Si or Al. These post-treatments lead either to the preservation of the parent structure by replacing directly Ge by Si or Al [10–12] or to the creation of new structures that usually have smaller pores [13,14].

IM-12 silicogermanate (framework type UTL) is formed by layers connected to each other through d4r units [9], with interconnecting 12 MR and 14 MR channels. Thus, the stabilization of this zeolite is highly motivating. The different applied post-treatments usually led to the formation of new structures like COK-14 [14], IPC-2 [15], IPC-4 [15], IPC-6 [16], IPC-7 [16], IPC-9 [17] and IPC-10 [17] with smaller pores. While Shamzy et al. [18] obtained the aluminated germanosilicate form of UTL, the treatments led to a decrease of the initial microporous volume from 0.21 to 0.14 $cm^3.g^{-1}$. Hence, stabilizing this silicogermanate through its transformation into its aluminosilicogermanate or aluminosilicate analogue while maintaining its initial microporous volume and crystallinity is a remaining scientific challenge.

Recently, our group showed using DFT calculations that substitutions of Ge by Al or Si using chloride molecules in gaseous phase are thermodynamically feasible for all silicogermanates [5]. Experimentally, such gaseous treatment has never been undertaken for the stabilization of silicogermanates in mild conditions. In this work, we used chloride molecules as substitution sources and developed a two-step treatment approach combining $SiCl_4$ gaseous and polyaluminum chloride (PAC) aqueous treatments and succeeded in converting the parent IM-12 silicogermanate into a new stable aluminosilicogermanate referred here as IZM-7 (IFPEN zeolitic material-number 7), with negligible loss of the initial microporosity and crystallinity. Various elemental and physicochemical techniques (XRD, N_2 physisorption, XRF, FTIR and ^{27}Al MAS NMR) were implemented to characterize the materials along the treatment procedure. IZM-7 aluminosilicogermanate was converted to a bifunctional catalyst by incorporation of Pt and was evaluated for the hydroisomerization of *n*-decane. Compared to conventional aluminosilicates such as the USY zeolites [19], the obtained new material showed a highly promising catalytic activity.

Results and discussion

All experimental details are reported in the supplementary materials. X-ray diffractometry (XRD) patterns in Figure 1 show that the initial UTL structure is maintained [9] even after water washing when the calcined sample is treated using $SiCl_4$ in gaseous form (giving the IM-12_Si sample), while in absence of this treatment the structure collapses (Figure S1). The structure was largely preserved after further treatments to incorporate aluminum using aqueous polyaluminum chloride solution (PAC treatments) giving the IZM-7 zeolite, Figure 1.

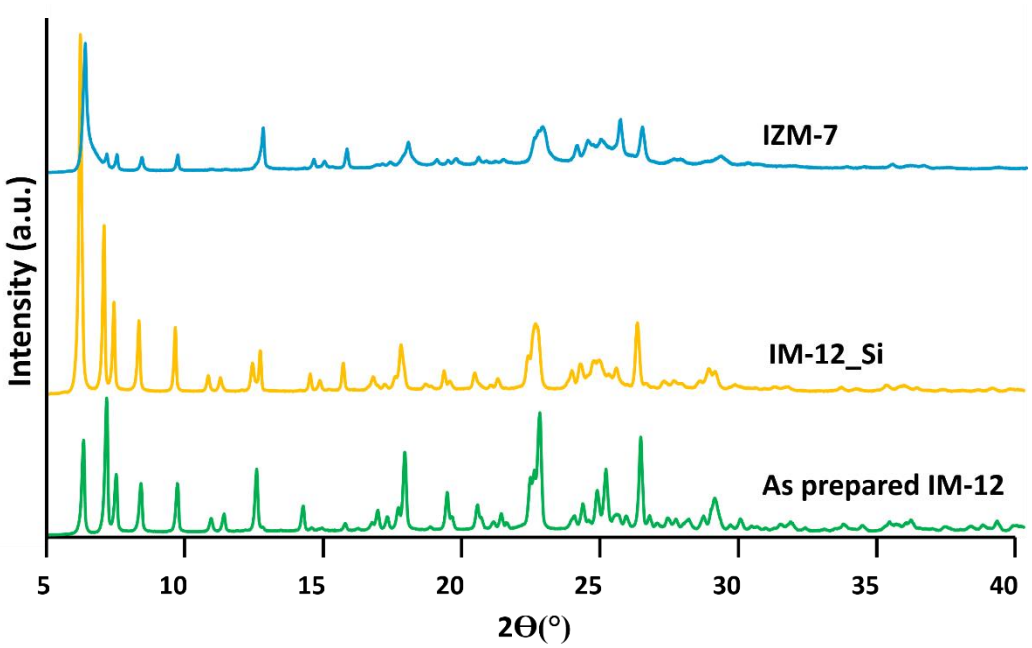

Figure 1: XRD patterns of as prepared IM-12, IM-12 treated with $SiCl_4$ (IM-12_Si) and IZM-7.

N_2 physisorption (Figure S2 and Table S1) shows that after the $SiCl_4$ treatment, 10% of the initial microporous volume is lost. After PAC treatment, this loss is reduced to 5% in the IZM-7 zeolite. The Brunauer, Emmett, Teller (BET) surface area follows the same trend, a decrease from 592 to 553 m^2/g in the IM-12_Si was detected before being quasi-restored (566 m^2/g) after the PAC treatment. This suggests that the IZM-7 and the aluminated germanosilicate reported by Shamzy et al. [18] are both stable. The difference between these samples is that the IZM-7 had higher microporous volume. This might indicate that the $SiCl_4$ gaseous treatment before the aqueous treatment led to an increase of the stability of the material, justifying the higher microporous volume even after further aqueous treatments. Scanning Electron Microscopy (SEM) pictures (Figure 2) show that the different treatments did not change the morphology and the size of the platelets. The basal plane average size is still around 7x6 μm and the average thickness around 350 nm. Moreover, the chemical mapping using energy dispersive X-ray spectroscopy (EDS) in annular dark-field scanning transmission electron microscopy (ADF-STEM) in Figure S3 reflect

a good dispersion of the Al along the crystal. X-ray fluorescence (XRF) shows an increase of the Si/Ge molar ratio from 5 in the parent IM-12 silicogermanate to 10 in the IM-12_Si sample. This increase is sufficient to stabilize the material. In IZM-7 zeolite, the Si/Ge molar ratio further increased to 173 while the Si/Al molar ratio was 27. The Attenuated Total Reflectance Infrared spectroscopy, ATR-IR spectra (Figure S4 and Table S1) of the as prepared IM-12 and of the treated samples agree with the XRF results. Only the as prepared sample has a band at 900 cm^{-1} attributed to Ge-O-Ge [20]. The absence of this band in the treated samples is consistent with the increase of the Si/Ge molar ratio from 5 to 10 after the $SiCl_4$ treatment and to 173 after the PAC treatments. Moreover, the band at 950 cm^{-1} attributed to asymmetric stretching vibration of Si-O-Ge in the framework [20,21] decreased with the increase of the Si/Ge molar ratio after the treatments. In addition, the shift of the band at 1054 cm^{-1} in the IM-12_Si to 1043 cm^{-1} in the IZM-7 suggests the incorporation of Al in the framework. The band characteristic of the vibration of d4r units [20,21] around 580 cm^{-1}, is present in all samples proving that these building units remained after the treatments and justifying the upholding of the UTL structure seen in the XRD patterns. This band presented a shift from 570 cm^{-1} in the as prepared IM-12 to $\simeq$ 582 cm^{-1} after the treatments suggesting that Ge was replaced by other elements in the d4r. A similar blueshift of 23 cm^{-1} was seen when Ge was substituted with Si in d4r units [21].

In addition, the ^{27}Al MAS NMR (Solid-state nuclear magnetic resonance) spectra represented in Figures S5 and S6 confirmed the incorporation of aluminum in the IZM-7 sample, and the beneficial effect of HCl washing on the Al_{VI} content. Al-content was determined based on the total Al area and the calculated Si/Al ratio of 31.4 was quite close to the Si/Al ratio 27 determined by XRF (Tables S1 and S3). The incorporated Al exist in 4 up to 6-coordinated environments, indicating that not all Al in the sample is incorporated in the zeolite framework. Zeolitic Al should

exist in tetrahedral coordination. Spectral decomposition revealed the presence of multiple tetracoordinated aluminum resonances with δ_{iso} around 57.3, 52.6 and 49.6 ppm and also multiple distributions of penta- (or distorted tetra-) and hexa-coordinated aluminum (Figure S6 and Tables S2 and S3). The resonance around 57.3 (T1) and 52.6 (T2) ppm can be assigned to Al incorporated in the zeolite framework [10,22,23] while the resonance at 48 ppm (DT) is considered as distorted tetra coordinated aluminum, that can be part of the zeolite framework or defect sites [24]. Si/Al^{IV} calculated based on total tetra-coordinated Al (T1 + T2) was 82 (200 μmol Al. g^{-1} zeolite). Estimated Si/Al ratio based on the two tetra-coordinated Al, *viz.*δ_{iso} = 57.3 ppm (T1) and δ_{iso} = 52.6 ppm (T2) resonances were 146 (equivalent to 113 μmol. g^{-1} of Al^{IV}) and 190 (equivalent to 87 μmol.g^{-1} of Al^{IV}) ppm respectively (Figure S6, Tables S2 & S3). Around 61 % of the incorporated Al is in distorted tetra-, penta- or hexa- coordination indicating the formation of amorphous Al deposits in the zeolite crystals.

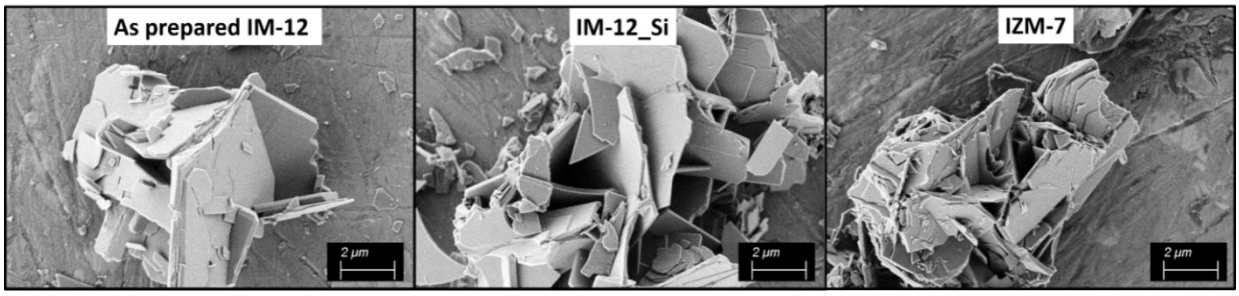

Figure 2: SEM images of as prepared IM-12, IM-12 treated with $SiCl_4$ (IM-12_Si) and IZM-7.

The nature of the hydroxyl groups in the calcined IM-12 and the post-treated samples was studied using Fourier transform infrared (FTIR) spectroscopy. The calcined IM-12 exhibits a peak around 3742 cm^{-1} attributed to silanols [18,25,26] and a large band between 3685-3630 cm^{-1} attributed to germanols [22]. As seen in Figure S7, after the $SiCl_4$ treatment the band characteristic of germanols decreased while the amount of silanols in the latter sample increased (from 94 to 330 μmol. g^{-1}). This might indicate that some germanols were replaced by silanols in addition to the creation of

some defects in the structure. Moreover, for the IZM-7 sample two new bands appeared, first a band at 3670 cm^{-1} assigned to EFAL or surface Al-(H_2O) [27] and aluminols [25,28], while the weak band around 3629 cm^{-1} is assigned to bridging Si-(OH)-Al expected to behave as Brønsted acid sites. Thus, from the IR experiments, it can be concluded that we succeeded in introducing bridging OH groups in the structure, but in very low amounts.

Quantification of Brønsted acid sites (BAS) and Lewis acid sites (LAS) was performed via *in situ* FTIR investigation of temperature programmed adsorption – desorption (TPD) of pyridine at 150°C. Accessibility of pyridine to all the sites may be an issue, given the channel orientation in a UTL framework is parallel to the sheets, such that the pores are accessible only via the edges of the platelets, leading to longer penetration depths. However, Figure S8 shows that bridging Si-OH-Al (3629 cm^{-1}) are accessible to the pyridine since after contact with pyridine their corresponding band vanishes (although a remaining band at 3629 cm^{-1} may still be present, hidden behind a large band corresponding to perturbed O-H species), as well as that of most silanols. The FTIR spectrum after desorption at 150°C in Figure S9, shows a band at 1545 cm^{-1} (ring vibration of the C-C bonds of the pyridinium ion) indicating that these are BAS [22,23,25,29]. The band at 1455 cm^{-1} (vibration of C-C bond due to coordinated pyridine) reflect the presence of LAS [25,29]. The amounts of BAS and LAS are respectively 81 and 96 μmol. g^{-1}. The amount of BAS observed (81 μmol. g^{-1}) is quite comparable to the two types of Al^{IV} estimated from ^{27}Al NMR (113 μmol. g^{-1} T1 or 87 μmol. g^{-1} T2), but determining whether both types of Al^{IV} are incorporated in the frame or one is part of the zeolite and the other to amorphous alumina is difficult to deduce. Compared to other conventional zeolites, the amount of Brønsted acid sites is lower than non-steamed zeolites, for example, a ZSM-5 sample having a total Si/Al ratio of 40, was reported to exhibit 243 μmol. g^{-1} of BAS [30] while a reference USY zeolite (CBV-760 provided from

Zeolyst) with a Si/Al of 30 has 129 μmol. g^{-1} of BAS, Figure S10. This means that the IZM-7 is in a potentially interesting acidity range. Note that for this sample, the more pronounced decrease in the amount of BAS and LAS sites calculated from the pyridine desorption at higher temperatures (Table S4) reflects that some of the acid sites of the CBV-760 are stronger than those of IZM-7. In the other hand, the amount of BAS generated by PAC treatment (81 μmol.g^{-1}) is much higher compared to other alumination procedures in literature for all silica zeolite materials, revealing the higher efficiency of the reported alumination procedure [31,32]. For instance, BAS generated via alumination of all silica -COK-14 (generated via degermanation of IM-12) by Al-ALD (BAS 6.5 μmol. g^{-1}), thermal treatment with aluminum isopropoxyde (15 μmol. g^{-1}) and wet-ball milling with aluminum isopropoxyde - isopropanol (11 μmol. g^{-1}) were much less abundant than in the present case.

The obtained IZM-7 was tested for the hydroisomerization of n-decane. In addition, the IM-12 zeolite treated with $SiCl_4$ (IM-12_Si sample, which still has few amounts of Ge) was also tested to verify whether it is active or not in the absence of Al. An alkane hydroconversion catalyst requires a synergy between the noble metal (Pt), which does dehydrogenation of alkanes to alkenes and hydrogenation of alkenes to alkanes, and the Brønsted acid sites, which protonate the alkenes into alkylcarbenium ions, which undergo isomerization and cracking reactions. Hence the two zeolites were impregnated with platinum to convert to bifunctional catalysts. The ADF-STEM-EDS in Figure S3 reflects the dispersion of Pt at the surface of the zeolite with an average particle size of 10 nm. Their dispersion calculated following ref. [33] is thus 10%. The observed catalytic activity was compared to that of a traditional ultrastable Y zeolite (USY, commercial CBV-760 provided from Zeolyst) based hydroconversion catalyst, 0.5 wt.% Pt/USY (Si/Al of 30). *n*-decane conversion started around 119°C and 147°C for IZM-7 and USY respectively (Figure 3.a). The

temperature at 50% of conversion is an indicator of the mass activity of the zeolite. The Pt/IZM-7 zeolite achieved 50% conversion at 157°C, while the reference Pt/USY zeolite tested in the same conditions achieved 50% conversion at 210°C. In the case of Pt/IM-12_Si, *n*-decane conversion started only at very high temperatures (around 250°C), achieving 50% of conversion at 310°C. This result is similar to that of the Pt/IM-12 catalysts, however, the Pt/IM-12_Si did not collapse during the catalytic test while the calcined Pt/IM-12 did [34]. The low activity of Pt/IM-12_Si is likely due to the absence of Brønsted acid sites. Pt/IZM-7 is much more active compared to Pt/USY catalyst even though the IZM-7 has lower number of Brønsted acid sites (81 µmol. g^{-1}) compared to the Pt/USY (129 µmol. g^{-1}, Figure S10). The turnover frequency (TOF) values, calculated by Brønsted acid site (from the number of BAS quantified by pyridine desorption at 150°C) at 173°C (temperature of 5% of conversion of decane over Pt/USY) are 33.09 10^3 s^{-1} and 0.29 10^3 s^{-1} for sample Pt/IZM-7 and Pt/USY respectively. This highlights again the higher activity of the Pt/IZM-7 catalyst. According to the mechanism of hydroconversion of *n*-decane, skeletal isomerization is followed by cracking reactions [35]. It is evident from the plot of isomerization and cracking selectivity as a function of the conversion (Figure 3.b) that the major products in *n*-decane conversion over Pt/IM-12_Si are cracked (or hydrogenolysis) products. This is attributed to the absence of Brønsted acidity in the Pt/IM-12_Si silicogermanate, which makes the catalyst behave as a monofunctional metallic catalyst, rather than a bifunctional one. This indicates that the dominant reaction that takes place on Pt/IM-12_Si is hydrogenolysis to short chain alkanes, predominantly methane (Figure S11) confirming the need of an alumination step to generate Brønsted acid sites.

The yield of the skeletal isomers against the *n*-decane conversion is presented in Figure 3b. The Pt/IZM-7 catalyst has lower selectivity for the decane isomers, compared to the Pt/USY catalyst,

46% vs 68% at maximum isomerization. The latter result can be related to morphological difference between the two zeolites since the IZM-7 has a 2D channel system vs. a 3D channel system in the USY. In addition, the bigger crystal size in the IZM-7 (7x6 µm and 350 nm of thickness) vs. 0.5-0.8 µm in the USY (Figure S12), may lead to a longer diffusion path resulting in an increase of the secondary cracking reactions. Moreover, the presence of mesopores in the USY crystals increases the accessibility to the active sites. The distribution of cracked product yields divided according to carbon numbers for IZM-7 (Figure S11) is fairly symmetric showing that molecules undergo cracking only once (C10 to two C5 molecules or C4 + C6 or C3 + C7), the first two pathways being the most preferred for IZM-7. Negligible formation of C1, C2, C8 and C9 fractions reveals the absence of hydrogenolysis reactions, confirming a good balance of the two functionalities, *viz.* noble metal and BAS in the 0.3wt% Pt/IZM-7 catalyst.

The distribution of ethyloctanes (EC8) and methyl nonanes (MC9) at 5% conversion can be used to distinguish between different pore architectures. In the case of IZM-7, the yield of EC8 vs. MC9 plot (Figure S13) suggests characteristic features of a 12MR pore architecture, to be compared with the expected 12MR-14MR architecture for UTL [34]. This could be due to slight blockage of the 14MR pores by amorphous aluminum deposit, which is present as indicated by ^{27}Al NMR. Another way of characterizing the pore architecture is the refined constraint index (CI*), which is defined as the ratio of the yields of 2-methylnonane to 5-methylnonane at 5% conversion. The presence of 12-MRs is indicated by a CI* value between 1 - 2.5, while 10-MRs have CI* values greater than 2.5. The CI* values of Pt/IZM-7 was 2.05 pointing towards a 12-MR like pore architecture, again could be attributed to partial pore blockage. This blockage may be avoided by further optimization of the alumination and acid washing treatment. Notably, the acid washing already performed has a strongly beneficial effect on the selectivity pattern (Figure S14), and on

the CI* value (before washing by HCl: 2.82, typical of 10MR architectures). Nevertheless, IZM-7 is a promising catalyst for hydroconversion reactions, but detailed investigations may be required for understanding the nature, location and behavior of the active sites. Notably, the IZM-7 sample exhibits higher LAS content (96 µmol. g^{-1}) with respect to the USY zeolite (29 µmol. g^{-1}), as determined by pyridine adsorption (spectra in Figures S9 and S10). The main difference between IZM-7 and USY in terms of LAS is the abundance of weak LAS in IZM-7 (Table S4). One may wonder whether a synergy between Brønsted and those Lewis acid sites, reported in the literature for alkane cracking [36–38], would be at the origin of the higher catalytic activity of the Pt/IZM-7 catalyst.

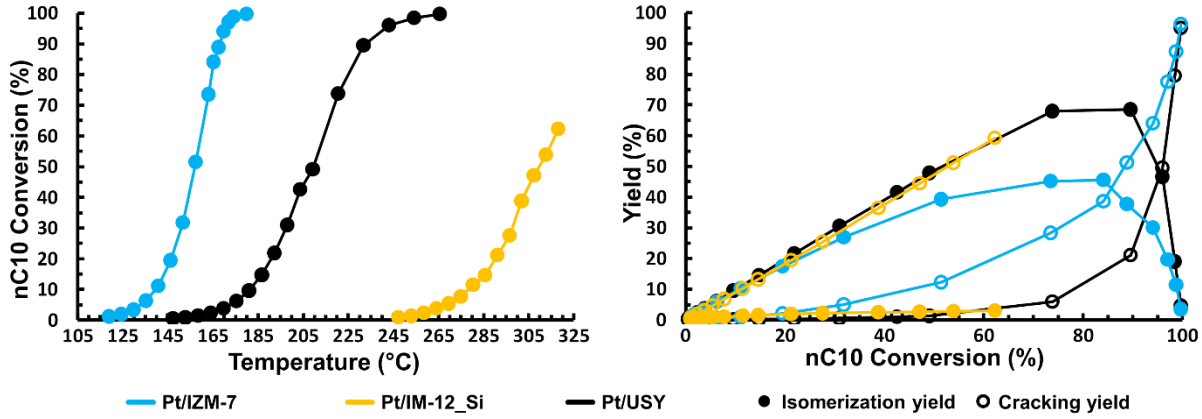

Figure 3:a) Conversion of n-decane against reaction temperature, (b) yield of n-decane skeletal isomers and cracked products against n-decane conversion, of the 0.3 wt.% Pt/IM-12_Si, 0.3 wt.% Pt/IZM-7 and 0.5wt.%Pt/USY catalysts.

To conclude, the stabilization of the IM-12 silicogermanate through the substitution of Ge by Si was for the first time performed by a treatment using $SiCl_4$ in gas phase in mild conditions. This treatment may additionally overcome the expensive cost of silicogermanates synthesis since the extracted Ge may be recovered and recycled for other syntheses [39]. After an optimization study of the different treatments, and for the first time to our knowledge, aluminum was incorporated

into this zeolite using the polyaluminum chloride (PAC) aqueous treatments without significant changes in its initial structure or its microporous volume. As a result, a new stable aluminosilicogermanate IZM-7 is obtained. Even considering the low amounts of acid sites, the IZM-7 zeolite presents an enhanced catalytic activity compared to conventional zeolites. Notably, instead of aluminum, the described methodology is promising to insert other kinds of Lewis acid cations in the framework of silicogermanate, expanding the possible application ranges of the materials [40,41]. Thus, this work opens new routes for the preparation of large pore active solids from inert frameworks, with tremendous expected consequences on reactivity and selectivity for many acid-catalyzed reactions (isomerization/cracking of hydrocarbons, methanol-to-olefin reactions, alcohol dehydration, sugar transformation, etc.), catalysis of oxygenated compounds on Lewis-acid sites, as well as for storage applications, due to the large pores of the silicogermanate structures.

Acknowledgments

E. Llido, V. Lefebvre, T. Coquet, (IFPEN), and Nicolas Bats (formally IFPEN, now Johnson Matthey) are acknowledged for experimental help and fruitful discussions. J.A.M acknowledges the Flemish government for long term structural funding (Methusalem) and the European Research Council (ERC) for an Advanced Research Grant under the European Union's Horizon 2020 research and innovation program under grant agreement No. 834134 (WATUSO). NMRCoRe acknowledges the Flemish government, department EWI for infrastructure investment via the Hermes Fund (AH.2016.134) and for financial support as International Research Infrastructure (I001321N: Nuclear Magnetic Resonance Spectroscopy Platform for Molecular Water Research).

References

[1] E.M. Gallego-Sánchez, M.T. Portilla, C.Paris, A. León-Escamilla, M. Boronat, M. Moliner, A. Corma, Science 355 (2017) 1051–1054.
[2] L. Bacakova, M. Vandrovcova, I. Kopova, I. Jirka, Biomater. Sci. 6 (2018) 974–989.
[3] N. Yu, R.Z. Wang, L.W. Wang, Prog. Energy Combust. Sci. 39 (2013) 489–514.
[4] T. Ennaert, J. Van Aelst, J. Dijkmans, R. De Clercq, W. Schutyser, M. Dusselier, D. Verboekend, B.F. Sels, Chem. Soc. Rev. 45 (2016) 584–611.
[5] E. El Hayek, B. Harbuzaru, J.A. Martens, C. Chizallet, Microporous Mesoporous Mater. 306 (2020) 110425–110434.
[6] M. Opanasenko, M. Shamzhy, Y. Wang, W. Yan, P. Nachtigall, J. Čejka, Angew. Chem. Int. Ed. 59 (2020) 2–12.
[7] J. Sun, C. Bonneau, A. Cantín, A. Corma, M.J. Díaz-Cabañas, M. Moliner, D. Zhang, M. Li, X. Zou, Nature 458 (2009) 1154–1157.
[8] A. Corma, M.J. Díaz-Cabañas, J.L. Jordá, C. Martínez, M. Moliner, Nature 443 (2006) 842–845.
[9] J.-L. Paillaud, B. Harbuzaru, J. Patarin, N. Bats, Science 304 (2004) 990–992.
[10] F. Gao, M. Jaber, K. Bozhilov, A. Vicente, C. Fernandez, V. Valtchev, J. Am. Chem. Soc. 131 (2009) 16580–16586.
[11] H. Xu, J. Jiang, B. Yang, L. Zhang, M. He, P. Wu, Angew. Chem. Int. Ed. 53 (2014) 1355–1359.
[12] A. Rodríguez-Fernández, F.J. Llopis, C. Martínez, M. Moliner, A. Corma, Microporous Mesoporous Mater. 267 (2018) 35–42.
[13] P. Eliášová, M. Opanasenko, P.S. Wheatley, M. Shamzhy, M. Mazur, P. Nachtigall, W.J. Roth, R.E. Morris, J. Čejka, Chem. Soc. Rev. 44 (2015) 7177–7206.
[14] E. Verheyen, L. Joos, K. Van Havenbergh, E. Breynaert, N. Kasian, E. Gobechiya, K. Houthoofd, C. Martineau, M. Hinterstein, F. Taulelle, V. Van Speybroeck, M. Waroquier, S. Bals, G. Van Tendeloo, C.E.A. Kirschhock, J.A. Martens, Nat. Mater. 11 (2012) 1059–1064.
[15] W.J. Roth, P. Nachtigall, R.E. Morris, P.S. Wheatley, V.R. Seymour, S.E. Ashbrook, P. Chlubná, L. Grajciar, M. Položij, A. Zukal, O. Shvets, J. Cejka, Nat. Chem. 5 (2013) 628–633.
[16] P.S. Wheatley, P. Chlubná-Eliášová, H. Greer, W. Zhou, V.R. Seymour, D.M. Dawson, S.E. Ashbrook, A.B. Pinar, L.B. McCusker, M. Opanasenko, J. Čejka, R.E. Morris, Angew. Chem. Int. Ed. 53 (2014) 13210–13214.
[17] M. Mazur, P.S. Wheatley, M. Navarro, W.J. Roth, M. Položij, A. Mayoral, P. Eliášová, P. Nachtigall, J. Čejka, R.E. Morris, Nat. Chem. 8 (2016) 58–62.
[18] M.V. Shamzhy, P. Eliašová, D. Vitvarová, M.V. Opanasenko, D.S. Firth, R.E. Morris, Chem. Eur. J. 22 (2016) 17377–17386.
[19] J.A. Martens, E. Benazzi, J. Brendlé, S. Lacombe, R. Le Dred, Studies in Surface Science and Catalysis Elsevier Science B.V. 130 (2000) 293–298.

[20] Le Xu, M.K. Choudhary, K. Muraoka, W. Chaikittisilp, T. Wakihara, J.D. Rimer, T. Okubo, Angew. Chem. 131 (2019) 14671–14675.
[21] H. Xu, J. Jiang, B. Yang, L. Zhang, M. He, P. Wu, Angew. Chem. 126 (2014) 1379–1383.
[22] V. Kasneryk, M. Opanasenko, M. Shamzhy, Z. Musilová, Y.S. Avadhut, M. Hartmann, J. Čejka, J. Mater. Chem. A 5 (2017) 22576–22587.
[23] Z. Zhang, Y. Guo, X. Liu, J. Phys. Chem. C 121 (2017) 11568–11575.
[24] B. Vallaey, S. Radhakrishnan, S. Heylen, C.V. Chandran, F. Taulelle, E. Breynaert, J.A. Martens, Phys. Chem. Chem. Phys. 20 (2018) 13528–13536.
[25] M. Shamzhy, Ramos, F.S. de O. Ramos, Catal. Today 243 (2015) 76–84.
[26] M. Moliner, M. J. Díaz-Cabañas, V. Fornés, C. Martínez, A. Corma, J. Catal. 254 (2008) 101–109.
[27] L. Treps, C. Demaret, D. Wisser, B. Harbuzaru, A. Méthivier, E. Guillon, D.V. Benedis, A. Gomez, T.d. Bruin, M. Rivallan, L. Catita, A. Lesage, C. Chizallet, J. Phys. Chem. C 125 (2021) 2163–2181.
[28] N.-Y. Topsøe, K. Pedersen, E.G. Derouane, J. Catal. 70 (1981) 41-52.
[29] C.A. Emeis, J. Catal. 141 (1993) 347–354.
[30] E. Verheyen, C. Jo, M. Kurttepeli, G. Vanbutsele, E. Gobechiya, T.I. Korányi, S. Bals, G. van Tendeloo, R. Ryoo, C.E. Kirschhock, J.A. Martens, J. Catal. 300 (2013) 70–80.
[31] E. Verheyen, S. Pulinthanathu Sree, K. Thomas, J. Dendooven, M. de Prins, G. Vanbutsele, E. Breynaert, J.-P. Gilson, C.E.A. Kirschhock, C. Detavernier, J.A. Martens, Chem. Commun. 50 (2014) 4610–4612.
[32] M. de Prins, E. Verheyen, G. Vanbutsele, S.P. Sree, K. Thomas, J.-P. Gilson, J. Vleugels, C.E. Kirschhock, J.A. Martens, Catal. Today 334 (2019) 3–12.
[33] S.P. Sree, J. Dendooven, P.C.M.M. Magusin, K. Thomas, J.-P. Gilson, F. Taulelle, C. Detavernier, J.A. Martens, Catal. Sci. Technol. 6 (2016) 6177–6186.
[34] N. Kasian, G. Vanbutsele, K. Houthoofd, T.I. Koranyi, J.A. Martens, C.E.A. Kirschhock, Catal. Sci. Technol. 1 (2011) 246–254.
[35] J.A. Martens, R. Parton, L. Uytterhoeven, P.A. Jacobs, Appl. Catal. 76 (1991) 95–116.
[36] R.M. Lago, W.O. Haag, R.J. Mikovsky, D.H. Olson, S.D. Hellring, K.D. Schmitt, G.T. Kerr, The Nature of the Catalytic Sites in HZSM-5- Activity Enhancement, Stud. Surf. Sci. Catal. (1986) 677–684.
[37] S. Schallmoser, T. Ikuno, M.F. Wagenhofer, R. Kolvenbach, G.L. Haller, M. Sanchez-Sanchez, J.A. Lercher, J. Catal. 316 (2014) 93–102.
[38] S.M.T. Almutairi, B. Mezari, G.A. Filonenko, P.C.M.M. Magusin, M.S. Rigutto, E.A. Pidko, E.J.M. Hensen, ChemCatChem 5 (2013) 452–466.
[39] J. Zhang, Q. Yue, M. Mazur, M. Opanasenko, M.V. Shamzhy, J. Čejka, ACS Sustainable Chem. Eng. 8 (2020) 8235–8246.
[40] T. Ennaert, J. van Aelst, J. Dijkmans, R. de Clercq, W. Schutyser, M. Dusselier, D. Verboekend, B.F. Sels, Chem. Soc. Rev. 45 (2016) 584–611.
[41] M. Moliner, Dalton Trans. 43 (2014) 4197–4208.